1   **Title: The Social Networks of Neural Progenitor Cells**

2

3   Authors: Arun Mahadevan[a], Jacob T. Robinson[a,b], Amina Ann Qutub[a*]

4

5   Author Affiliations:

6   [a]Department of Bioengineering, Rice University, Houston, TX 77030

7   [b]Department of Electrical and Computer Engineering, Rice University, Houston, TX 77030

8

9   [*]Corresponding Author

10

11   Amina A. Qutub

12   Assistant Professor, Department of Bioengineering

13   Rice University

14   BioScience Research Collaborative

15   6500 Main St., Rm 613

16   Houston, TX 77030

17   Office: (713) 348-8089 / Cell: (510) 541-3497

18   Email: aminaq@rice.edu

19

20

21

22

23

24

25   **Abstract**

26

27   Quantitative understanding of how neural progenitor cells (NPCs) collectively self-organize into neural

28   networks can provide critical insight into how to optimize neural regenerative strategies. To that end, we

29   characterized the topology of human embryonic NPCs during differentiation by designing and employing

30   a spatial graph-theoretic analysis. Statistical measures of information flow in NPC spatial graphs revealed

31   a shift from topologies with high global efficiency to high local efficiency, around the time mature

32   neuronal phenotypes appeared in culture. These results support the view that network-wide signaling in

33   immature progenitor cells gives way to a more structured, hierarchical form of communication in mature

34   neural networks. We also demonstrate that the evaluation of recurring motif patterns in NPC graphs

35   reveals unique geometric arrangements of cells in neural rosette-like structures at early stages of

36   differentiation. Our approach provides insight into the design of developing neural networks, opening the

37   door for new approaches that modulate neural cell self-organization for therapeutic applications.

38

39   Human embryonic stem cells (hESCs) and other sources of pluripotent stem cells have provided much

40   hope for regenerative medicine, especially in the nervous system (Fred H. Gage and Temple 2013).

41   Recently, stem cell therapies have been reported to treat neurological disorders, including stroke and

42   neurodegenerative diseases like Parkinson's disease (Hallett et al. 2014; Rosado-de-Castro et al. 2013). In

43   addition, neural progenitor cells derived from embryonic stem cells (hNPCs) and dissociated cultures

44   have helped elucidate intrinsic transcriptional control of self-renewal and multipotency (Guillemot 2007;

45   Imayoshi and Kageyama 2014; Shen et al. 2006; Kageyama et al. 2009). The influence of external cues

46   such as morphogen gradients in guiding nervous system development is also well documented (Mason

47   2007; Bertrand and Dahmane 2006). Aside from intrinsic genetic programs and extrinsic cues, a third

48   aspect of stem cell differentiation that merits further study is the collective self-organization of progenitor

49   cells into functional neural networks. Quantitative insight into neural cell self-organization, in addition to

50   knowledge of external and intrinsic cues that guide tissue development, will ultimately be necessary to

51   design effective and targeted stem cell therapies.

52

53   Cell-cell communication among progenitor cells is an essential aspect of nervous system development.

54   Neural progenitor cells cluster together in specialized microenvironments or niches where communication

55   with neighboring cells plays an important role in determining cell behavior (ffrench-Constant 2008). Prior

56   to the formation of functional synapses, NPCs display structured intercellular communication that plays a

57   critical role in the spatiotemporal control of self-renewal and differentiation, and also shapes developing

58   neural circuits. Examples of structured cell-cell communication include patterned, spontaneous electrical

59   activity mediated partly through gap junctional coupling (Malmersjö et al. 2013; Spitzer 2006;

60   Blankenship and Feller 2010), maintenance of intercellular configurations through tight junction proteins

61   (Watters et al. 2015) and control of cell differentiation through Notch signaling (Edri et al. 2015;

62   Shimojo, Ohtsuka, and Kageyama 2008). Notably, the predominant forms of communication employed

63   by NPCs can be described as juxtacrine signaling, i.e., requiring direct cell-cell contact. Thus, the

64   immediate cellular neighborhood of a progenitor cell provides an important context in which to place its

65   dynamic behavior.

66

67   Live-cell imaging approaches have yielded significant insight into the dynamics of multipotent progenitor

68   cells, particularly when coupled with automated image analysis (Imayoshi et al. 2013; Schroeder 2011;

69   Cohen et al. 2010). However, most of these studies focus on cell-autonomous mechanisms that guide self-

70   renewal and differentiation of progenitor cells. Graph theory and network analysis methods are well

71   suited to uncover the role of structured communication among progenitor cells in guiding their behavior.

72   Graph-theoretic methods have been used to study functional and anatomical connectivity in the adult

73   brain, leading to significant insight into brain organization (Bullmore et al. 2009). A number of studies

74   have also applied graph-theoretic approaches to study the functional and anatomical connectivity of

75   cultured neuronal circuits (Feldt, Bonifazi, and Cossart 2011; Shefi, Ben-Jacob, and Ayali 2002; de

76   Santos-Sierra, Sendiña-Nadal, Leyva, Almendral, Anava, et al. 2014; Downes et al. 2012). However,

77   these studies are often conducted in dissociated cultures of post-mitotic neurons, where the physical

78   wiring among neurons is important and network-wide information is conveyed primarily through synaptic

79   contacts. Given the dominance of juxtacrine modes of signaling among progenitor cells, we reasoned that

80   adapting graph-theoretic approaches to study the spatial organization of neural progenitors during

81   differentiation would yield insight into the spatial evolution of progenitor cell communities and their

82   relationship with functional differentiation state.

83

84   Here we present a detailed characterization of spatial organization of H9-derived human neural progenitor

85   cells during neural differentiation over the course of 14 days. To achieve this characterization, we

86   introduce a new approach that integrates weeks-long live imaging assays, automated image analysis and a

87   graph-theoretic approach based on cell body proximity to quantify the spatial organization of progenitor

88   cells. A schematic representation of our experimental paradigm is shown in Figure 1. We use our method

89   to demonstrate that NPCs transition from topologies with high global efficiency to those with high local

90 efficiency for information flow around the time mature neuronal phenotypes appear in culture. We also

91 show that our graph-based metrics capture the characteristic geometric arrangement of cells in neural

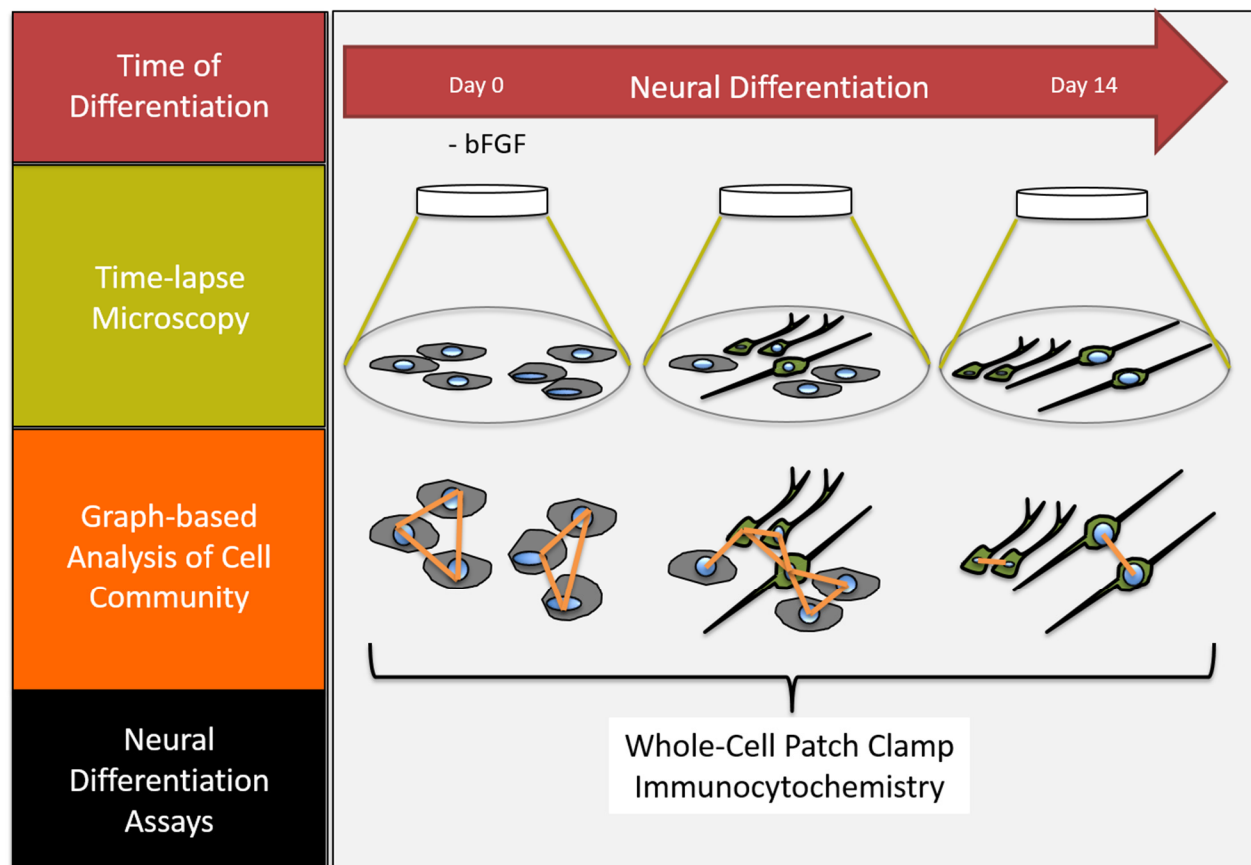92 rosette-like structures seen at early time points of differentiation.

Figure 1. Schematic illustrating the design of the experiments.

93   **Results**

94

95   **Functional characterization of differentiating hNPC cultures.** The model cell culture system used in

96   this study is neural progenitor cells derived from H9 human embryonic stem cells. These cells were
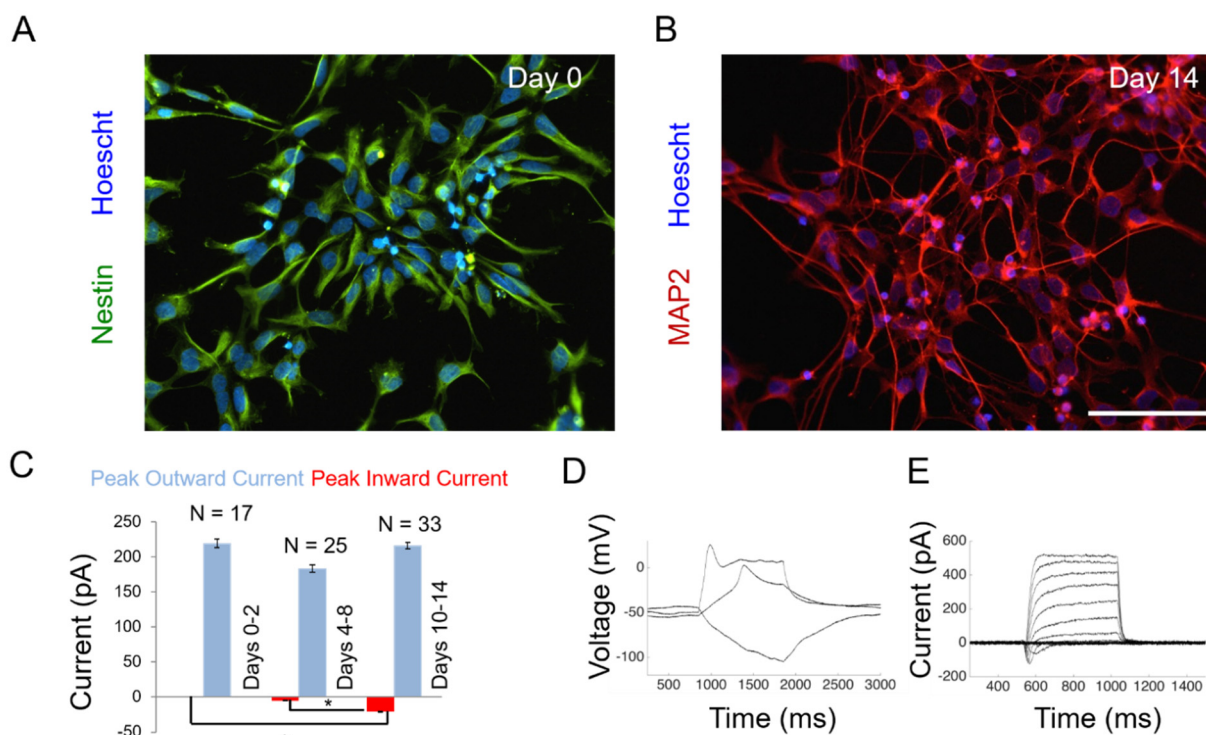

Figure 2. Functional characterization of differentiating hNPCs. (A) hNPCs at day 0 stain positively for Nestin. Nuclei are labeled by Hoescht. (B) Cells at day 14 stain positive for MAP2. Nuclei are labeled by Hoescht (scale bar = 100µm). (C) Peak inward and outward currents determined through whole-cell patch clamp electrophysiology. Number of cells recorded (N) is shown above the bar for each time period. Error bars represent S.E.M. Student t-test was performed for each pair of samples; * P<0.05. (D) Weak action potentials evoked from a cell at day 14 through current injection. Magnitudes of current injected are -30pA, +20pA and +120pA from holding. (E) Voltage-gated inward and outward currents seen in the same cell. Voltage steps applied were from -60mV to +90mV in 10mV increments.

97   maintained as undifferentiated, mitotic progenitor cells in the presence of the mitogen basic fibroblast

98   growth factor (bFGF). Withdrawal of bFGF from culture medium was used to induce spontaneous

99   differentiation of hNPCs (F. H. Gage 2000).

100

101   We performed immunocytochemistry and whole-cell patch clamp electrophysiology experiments to

102   uncover the time course of functional development in differentiating hNPCs. Cells at day 0 stained

103   positively for Nestin, a Type VI intermediate filament expressed by dividing neural progenitor cells

104   (Figure 2A). Cells at day 14 were positive for microtubule-associated protein-2 (MAP2), a protein

105   associated with dendrite formation in maturing neuronal cells (Figure 2B). Analysis of peak inward and

106   outward currents from voltage-clamp experiments showed that cells at all time points exhibited the same

107   levels of outward currents, but showed increasing magnitudes of inward currents (Figure 2C). Inward

108   currents are typically driven by voltage-gated sodium channels, and their presence indicates a more

109   mature neuronal phenotype. Furthermore, weak action potentials could be elicited from cells showing

110   inward currents at later time points (3/11 cells at day 14) through current injection. Sample current-clamp

111   and voltage-clamp traces are shown for a cell recorded at day 14 in Figure 2D and 2E. These experiments

112   showed that Nestin-positive hNPCs matured over 14 days to MAP2-positive neurons, with neuronal fate

113   commitment occurring between days 4-8 (indicated by the appearance of neuronal phenotypes in that time

114   period).

115

116   **Representation of cell community structure using a graph-based approach.** In order to uncover

117   topological changes in differentiating hNPCs, we combined long-term time-lapse microscopy of

118   differentiating cultures with a graph-based approach for quantifying cell community structure. We

119   conducted two biologically independent experiments where cultures were imaged at days 0, 3, 6, 9, 12

120   and 14 after withdrawal of bFGF. An additional dataset was obtained by imaging differentiating cultures

121   at 1-hour intervals for a total duration of 8 days (Supplemental Video 1). Selected image sequences were

122   analyzed using custom image-processing algorithms, resulting in the extraction of soma and neurites for

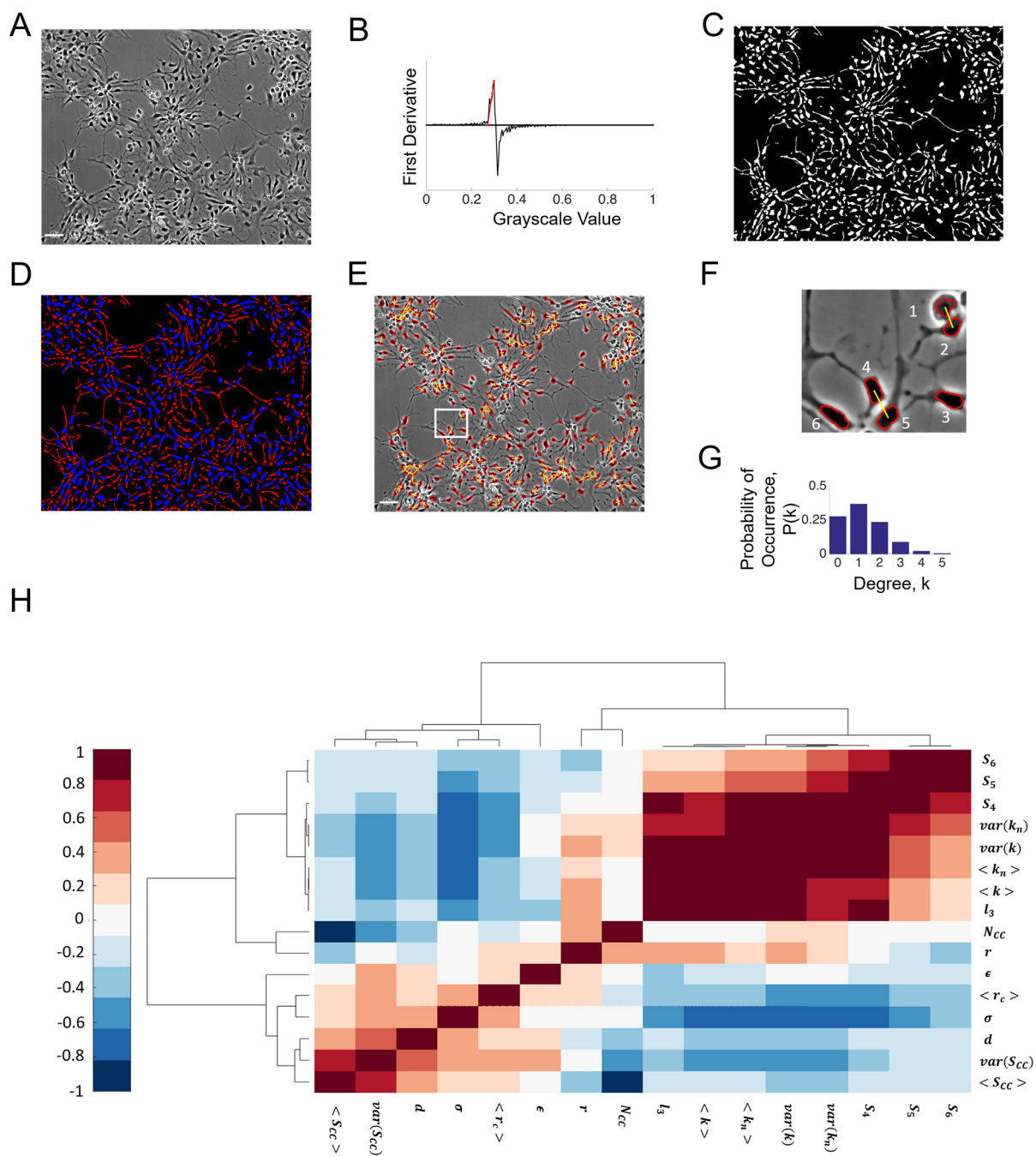123   each phase-contrast image (Figure 3A-D) (see Methods section for details).

124

Figure 3. Image processing and graph representation of time-lapse microscopy images.

(A) Representative grayscale image of human NPCs, shown at Day 3 (scale bar = 50 µm). (B) First derivative of the pixel intensity histogram, with a linear fit to the ascending portion shown as a red line. (C) Binary image obtained after thresholding is applied. (D) Separation of linear features through morphological opening of binary image yields cell bodies (blue) and neurites (red). (E) Phase contrast image with soma boundaries overlaid in red, and proximity edges shown in yellow. (F) Inset from panel A showing six soma, of which two pairs (1, 2) and (4, 5) are connected by proximity edges; the intercellular distance for these two pairs are smaller than their average diameter multiplied by a scaling factor S = 2; Soma 3 and 6 are isolated nodes since they are not sufficiently close to any other soma. (G) Degree distribution of the graph in panel E; number of nodes = 317, number of edges = 152, average degree, <k> = 0.96 (H) Correlation heatmap of all metrics obtained by hierarchical clustering of the covariance matrix.

125

126   neural circuits. In order to build quantitative representations of hNPC communities that reflect the modes

127   of communication employed by hNPCs, we developed a graph-based approach, where soma are denoted

128   as nodes and spatial proximity of cells is used to assign edges. In this manner, we constructed non-

129   weighted, undirected graphs representing hNPC communities from time-lapse microscope images

130   (Supplemental Video 2).

131

132   In order to describe the structure and topology of NPC community graphs, we evaluated a number of

133   metrics derived from graph theory. Table 1 lists 16 metrics that were computed, normalized appropriately

134   to account for network size (Bounova and De Weck 2012). The network metrics provide information on

135   various aspects of the graph structure such as information flow, connectivity and abundance of motifs.

136   Figure 3H shows the covariance matrix of all 16 metrics as a hierarchically clustered heatmap. The

137   heatmap shows several strong positive correlations among degree-related metrics like average degree,

138   average neighbor degree and their variances. Interesting negative correlations include that between

139   network efficiency and number of connected components, and those between clustering coefficient and all

140   degree-related metrics. In the following sections, we focus on metrics that have intuitive biological

141   interpretations, their trends across time of differentiation, and relationships observed with other metrics

142   that explain these trends. Trends in metrics not discussed in the main text are shown in Supplemental

143   Figure 4.

144

145   **Table 1. Metrics computed, their descriptions, and mode of normalization to account for**

146   **the network size. n = number of nodes, m = number of edges.**

Graph Metrics	Symbol	Definition	Normalization
Network Density	$< k >$	Average degree of graph, normalized by total maximum possible degree $$< k >= \frac{2m}{n(n-1)}$$	Maximum possible degree, $(n-1)$
Variance in Degree	$var(k)$	Variance of normalized node degree sequence	Node degree sequence normalized by maximum possible degree, (n-1)
Average Neighbor Degree	$< k_n >$	Average degree of node neighborhood, across all nodes	Maximum possible degree, (n-1)
Variance in Neighbor Degree	$var(k_n)$	Variance of the normalized average neighbor degree sequence	-
Network Efficiency	ϵ	The average reciprocal of shortest path length across all pairs of nodes, E	Average network efficiency of 100 random graphs generated through degree-preserving rewiring, E_{rand}. Random graph generation is illustrated in Fig. S3.
Average Clustering	σ	Fraction of total possible links among the	Average clustering

Coefficient		neighbors of a node that are actually present, averaged across all nodes, C	coefficient of 100 random graphs generated through degree-preserving rewiring, C_{rand}
Number of connected components	N_{CC}	Number of disconnected sub-graphs in main graph	-
Average Size of Connected Components	$<S_{CC}>$	Average number of nodes in each connected component	Total nodes, n
Variance in size of connected components	$var(S_{CC})$	-	-
Network Diameter	d	Longest shortest path length of network	Longest possible path, (n-1)
Triangular loop count	l_3	Number of loops of 3 nodes	Total possible number of triplets, $^nC_3$
4-star motif Count	S_4	Number of star motifs with one hub and three spokes	Total possible number of 4-tuples, $^nC_4$
5-star motif count	S_5	Number of star motifs with one hub and four spokes	Total possible number of 5-tuples, $^nC_5$
6-star motif count	S_6	Number of star motifs with one hub and five spokes	Total possible number of 6-tuples, $^nC_6$
Rich-Club Metric Average	$<r_c>$	Measure of the tendency of hub nodes (nodes with high number of links) to be well connected among each other (Colizza et al. 2006); Computed for threshold degrees between 1 and (n-1)	Average Rich-Club Metric of 100 random graphs generated through degree-preserving rewiring, RCM_{rand}
Assortativity	r	Pearson correlation coefficient of degrees between pairs of linked nodes (Newman 2002).	-

147

148   **Structure and information flow in NPC community graphs.** Network efficiency and clustering

149   coefficient are commonly used measures of efficiency in global and local information flow (see
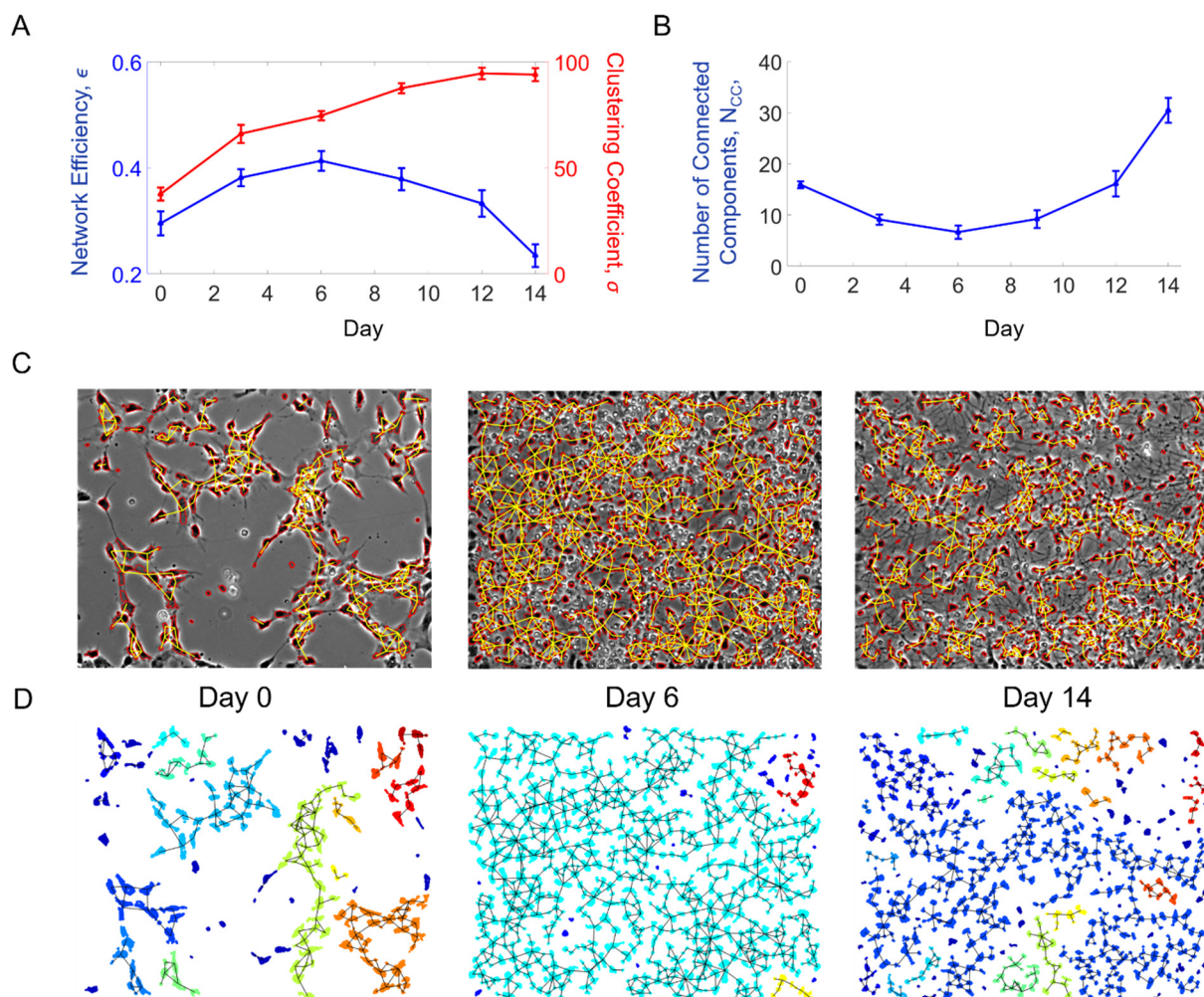

Figure 4. Metrics describing graph connectivity and information flow. (A) Network Efficiency (ϵ) and Clustering Coefficient (σ) across time. Note that the values reported are normalized by corresponding random graph values (see Table 1). (B) Number of connected components (N_{CC}) and network density ($< k >$) across time. (C) Graph representations of images taken at day 0, day 6 and day 14. Soma are outlined in red and edges are shown in yellow. (D) Cell bodies from the images in panel D, with each connected component labeled with distinct colors. Values are reported as the mean across N = 30 networks $\pm$ S.E.M

150   Table 1). When applied to the NPC networks, these metrics describe the efficiency of information

151   exchange at the network-wide and local neighborhood levels through cell body proximity

152   (compared to random graphs obtained through degree-preserving rewiring (Supplemental Figure

153   3)). In this context, information exchange could include flow of ions or growth factors between

154   cells through cell-adjacent means like gap junctions. Evaluation of these metrics in NPC networks

155   sampled across 30 different locations from two biologically independent experiments showed that

156   network efficiency increased from day 0 to day 6, and then decreased from days 6 to 14, while

157   clustering coefficient rose constantly from day 0 to 14 (Figure 4B). Thus, there appears to be a

158   transition from topologies favoring global information flow to those favoring a more structured,

159   hierarchical form of communication, occurring from day 6 – 14 of differentiation.

160

161   The correlation heatmap in Figure 3H shows a strong negative correlation between network

162   efficiency and number of connected components in the graph. The number of connected

163   components is a count of the number of disconnected sub-graphs in the main network and is a

164   measure of the connectivity of the graph – a graph with a high number of connected components

165   has a low connectivity. NPC networks at day 0, 6, and 14 are shown in Figure 4D and the

166   corresponding connected components are shown in Figure 4E. The formation of a giant connected

167   component due to cell proliferation up to day 6 leads to an increase in the connectivity of the

168   network, which in turn causes an increase in network efficiency. The subsequent disaggregation

169   of the large component into smaller modules from days 6 to 14 contributes to the decrease in

170   efficiency seen in that time period.

171 **Motif counts indicative of rosette-like topologies.** We observed relatively high motif counts

172 (star-patterns and loops) at early time points of culture (Supplemental Figure 4). Neuroepithelial

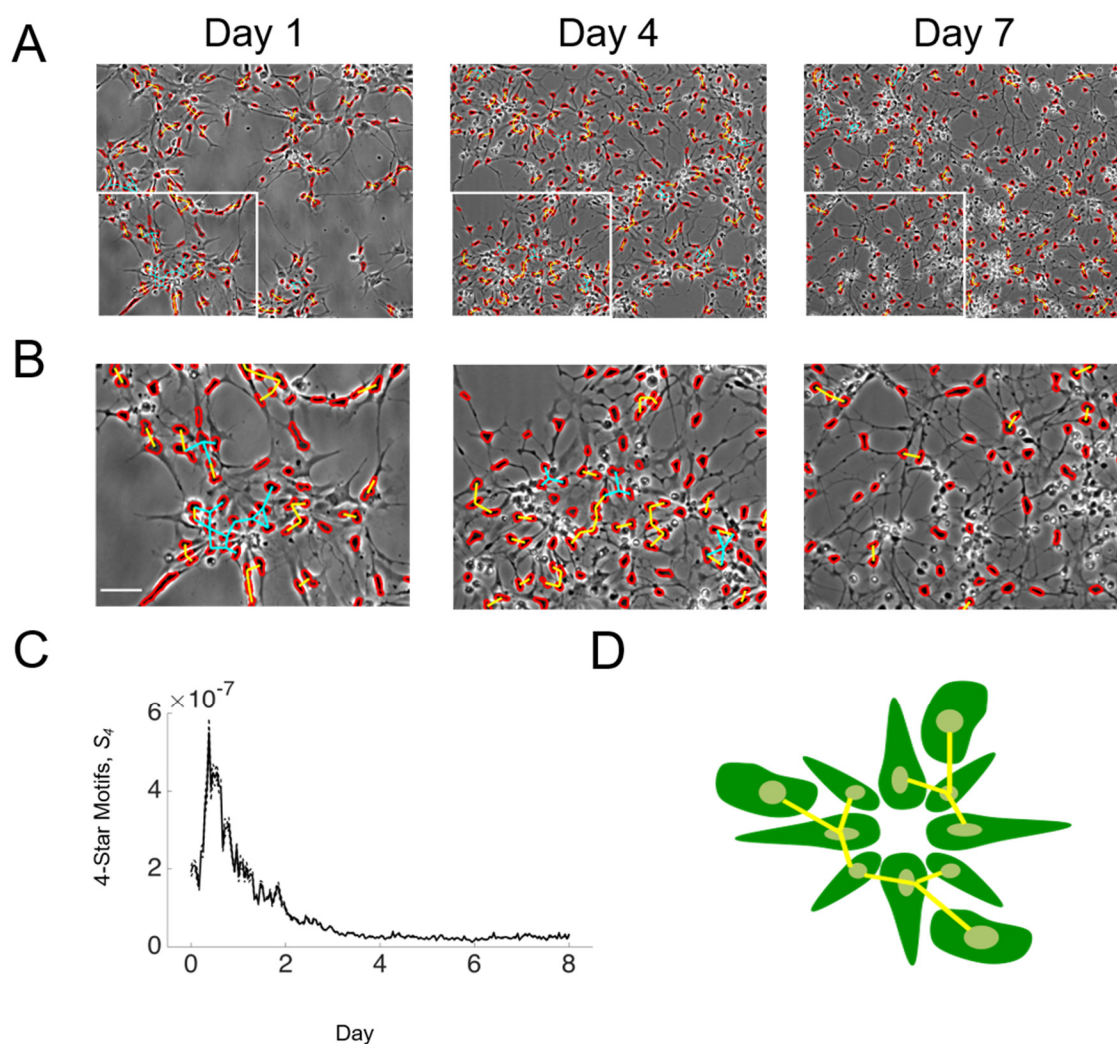173 cells are known to self-organize *in vitro* into rosette structures reminiscent of cross-sections of the

Figure 5. Motif counts indicate the presence of rosette-like structures. (A) Graph representations of NPC networks at day 1, 4 and 7; soma outlines are shown in red, proximity edges in yellow and edges part of a 4-star motif are highlighted in cyan. (B) Insets from corresponding images in panel A. (C) 4-star motif counts, normalized by the total possible 4-tuples. Note that 5-star and 6-star motif counts displayed similar trends (data not shown). (D) Schematic representation of rosette-like structures as a source of 4-star motifs. Values are reported as the mean across N = 10 networks ± S.E.M.

174   embryonic neural tube (Wilson and Stice 2006). We hypothesized that the high number of loops

175   and star-motifs at early time points was caused by rosette-like formations in culture. In order to

176   investigate this more closely, we collected an additional dataset where differentiating cultures

177   were continuously monitoring for 8 days at 1-hour intervals (Supplemental Video 1 and 2). We

178   observed radial arrangements of columnar cells 1-2 days after removal of bFGF followed by

179   disaggregation of these structures after day 4 (Figure 5A, 5B). 4-star motifs – topological patterns

180   with 1 central hub cell and 4 spoke cells – are highlighted in Figure 5B and the normalized counts

181   are shown in Figure 5C. 5- and 6-star motif counts showed similar trends (data not shown). Thus,

182   the relative abundance of high-degree motifs at early time points can be attributed to the unique

183   spatial arrangement of cells in a rosette-like structure (Figure 5D) and the low count at later time

184   points corresponds to the disaggregation of these structures and more regular arrangements of

185   cells.

186

Discussion

188   Because chemical and electrical signaling between neural progenitor cells often involves direct

189   contact between adjacent cells, we expect spatial cell organization to be an important aspect of

190   neural development. Two examples where spatial organization would play a role include the

191   Notch/Delta signaling and gap junctional communication between cells. The Notch/Delta

192   signaling pathway, which influences the proliferation and neuronal fate commitment of

193   progenitor cells (Zhou et al. 2010; Androutsellis-Theotokis et al. 2006), is an example of

194   juxtacrine chemical signaling. The canonical Notch signaling pathway functions through the

195   binding of a transmembrane ligand on one cell with the transmembrane receptor on a contacting

196   cell, resulting in the release of the notch intracellular domain (NICD) to initiate downstream

197   signaling cascades in the contacting cell (Andersson, Sandberg, and Lendahl 2011). In addition,

198   immature neural circuits are known to display spontaneous electrical activity, which is an

199   important aspect of their proper development (Spitzer 2006; Blankenship and Feller 2010). Gap

200   junctions or electrical synapses allow direct access between cells and result in exchange of ions

201   and growth factors, and these are known to be important in the propagation of spontaneous

202   electrical activity. Indeed, neural progenitor cells have been shown to display structured and

203   synchronous calcium activity, dependent on gap junctions and which promotes cell proliferation

204   (Malmersjö et al. 2013). More broadly, structured cell-cell communication has been implicated in

205   coordinated chemosensing (Sun et al. 2012) and migration during development (Friedl and

206   Gilmour 2009). Thus, the methods of cell-cell communication employed by immature neural cells

207   indicate the significance of spatially organized electrical and chemical signaling.

208

209   Our study provides quantification of the spatial organization of immature neural cells during

210   differentiation, using a unique application of graph theory. The experimental paradigm presented

211   here enabled us to uncover relationships between spatial topology of NPC communities and

212   functional maturation of developing neural circuits, and allowed us to develop hypotheses about

213   the role of certain topologies on NPC function. It is to be noted that not all metrics derived from

214   graph theory have a ready biological interpretation, especially in the context of spatial graphs. For

215   example, interpretation of metrics like degree-degree correlations and rich-club metric

216   (Supplemental Figure 4) are limited, due to the implicit limit in the type of connections that are

217   possible in spatial graphs. Keeping this in mind, we analyzed metrics with an intuitive biological

218   interpretation, i.e., information flow and connectivity.

219

220   We use our graph-based approach to analyze trends in information flow in NPC networks. Global

221   network efficiency rises from day $0 - 6$, and then falls from day $6 - 14$. The trend in network

222   efficiency is intuitively explained by its negative correlation with the number of connected

223   components, a measure of graph connectivity. Cell proliferation from day $0 - 6$ leads to the

224   merging of many disconnected clusters of cells into a giant connected component, leading to a

225   rise in the overall connectivity and reduction in the average path length. The reorganization of the

226   giant component into smaller modules from day 6 – 14 leads to a reduction in network efficiency.

227   Overall, our data indicates that the topologies observed at intermediate stages of differentiation

228   would facilitate cellular behavior requiring network-wide coordination, like chemosensing,

229   migration and proliferation (Figure 6).

230

231   We observed a constant rise in clustering coefficient, a measure of efficiency in local information

232   flow. Previous studies on dissociated cultures have shown the prevalence of clustering of neuron

233   cell bodies during maturation in culture (Shefi et al. 2002; de Santos-Sierra, Sendiña-Nadal,

234   Leyva, Almendral, Ayali, et al. 2014), indicating a common pattern in neuron self-organization

235   and wiring. High clustering facilitating local computations, accompanied by long-range neurite

236   connections to connect different clusters has been hypothesized to facilitate increased wiring

237   efficiency in mature neural circuits. The characteristic "small-world" network topology is also

238   hypothesized to be the organizing principle in the human brain (Bullmore et al. 2009). Thus, the

239   reorganization of cell bodies into highly clustered units in our study supports this view of

240   maturing neural circuits.

241

242   The fall of network efficiency and rise of clustering coefficient (compared to random networks)

243   from day 6 -14 indicates a shift from topologies favoring global information flow to those

244   favoring information flow in more restricted neighborhoods. It is interesting to note that this shift

245   occurs around the time mature neuronal phenotypes appear in culture. We believe this indicates a

246   shift in the mode of communication from network-wide signaling to a more structured,

247   hierarchical form of communication in mature neuronal networks. As discussed previously,

248   network-wide communication is implicated in facilitating behaviors like cell proliferation,

249   migration and coordinated chemosensing, while the reorganization of more mature neuronal

250   cultures into highly clustered cell bodies likely serves the purpose of increasing the wiring

251   efficiency. Conceptually, these ideas are represented in the schematic in Figure 6.

252

253   Our method also detected the formation of neural rosette-like structures. Neural rosettes are

254   known to harbor specific phenotypes such as apico-basal polarity, active Notch signaling and

255   interkinetic nuclear migration, all of which are involved in the proper sequential production of

256   neurons and glia (Abranches et al. 2009; Wilson and Stice 2006). We found that high-degree star-

257   motifs (comprising of a hub cell with 4-6 spoke cells) were present in high numbers at early time
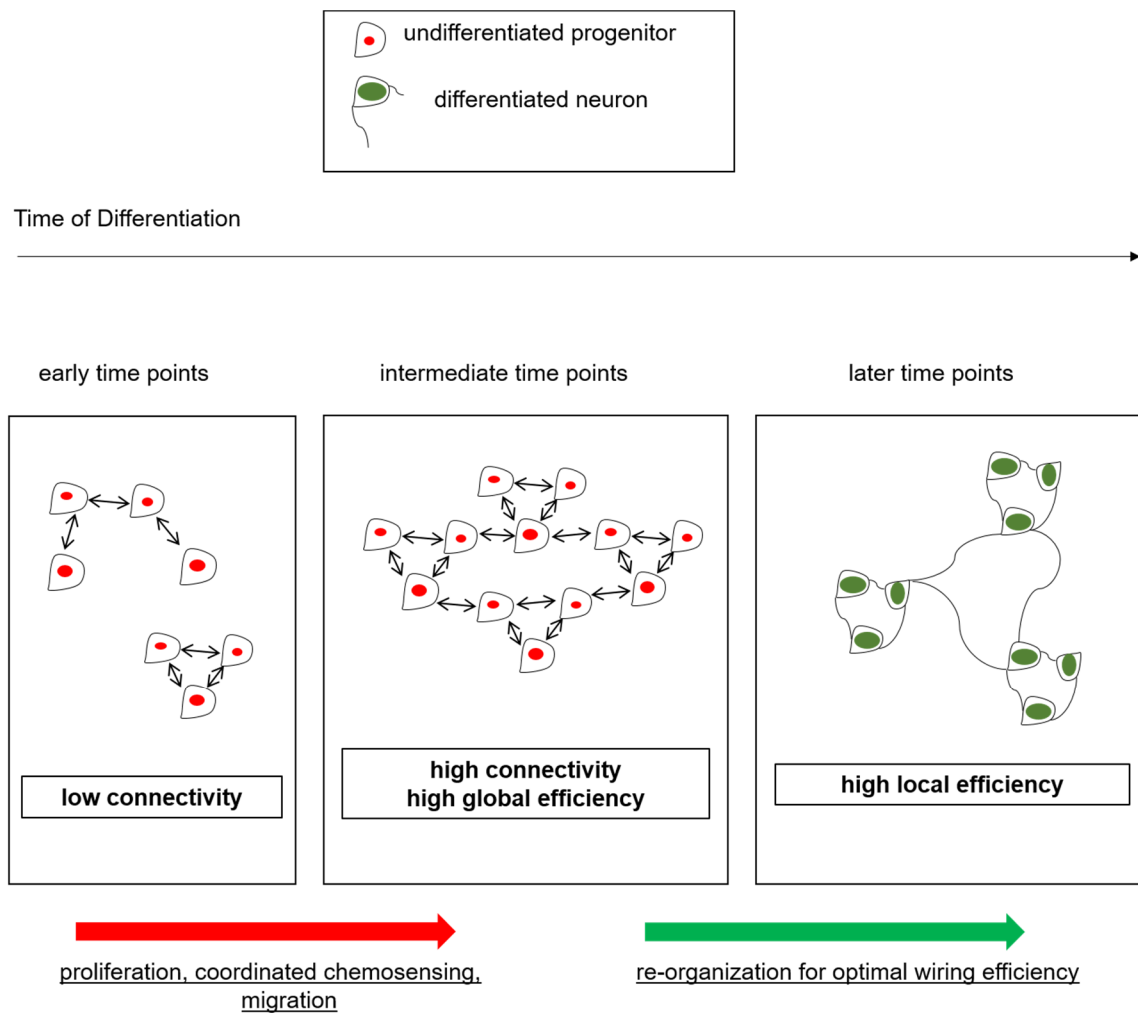

Figure 6. Schematic illustrating the observed changes in neural cell information flow during differentiation.

258   points (within 1-2 days of the differentiation stimulus) due to the unique geometric arrangement

259   of cells forming rosette-like structures. We also observed a decrease in star-motif counts

260   corresponding with the disaggregation of these structures after day 4. These results further

261   highlight the useful biological information that can be obtained through topological analysis of

262   differentiating hNPCs.

263

264   In this study, we show that network analysis provides unique information about the structure of

265   neural progenitor cell communities at the local and global levels. It remains to be seen whether

266   spatial topology of developing cultures is predictive of synaptic connectivity in mature neuronal

267   networks. Several *in vivo* studies have provided evidence for a structure-functional relationship

268   between adult neuronal wiring and the spatiotemporal origin of the constituent neurons. For

269   example, sister excitatory neurons in the neocortex are more likely to develop synapses with each

270   other rather than with other cells (Yu et al. 2009), and the electrophysiological phenotypes of

271   GABAergic interneurons have been shown to be dependent on the time and place of their birth

272   (Butt et al. 2005). Thus, the analysis of spatial topology in developing neuronal circuits in a

273   controlled setting has the potential to uncover structure-function relationships in the resulting

274   mature neural circuits.

275

276   The present study also lays the foundation for analysis of the role of cellular neighborhood on cell

277   fate determination of individual progenitor cells. The expression of cell-fate determination factors

278   such as bHLH transcription factors like Hes1 and Ngn2, and proteins involved in cell-cell

279   communication pathways such as Notch/Delta proteins, have been shown to be tightly coupled

280   with each other (Shimojo, Ohtsuka, and Kageyama 2008; Kageyama et al. 2009). Computational

281   modeling studies have predicted that Notch-Hes1 intercellular signaling affects differentiation

282   and cell cycle progression of individual cells and this signaling is important for the maintenance

283   of an optimal balance between differentiating cells and self-renewing progenitor cells (Pfeuty

284   2015). The spatial dynamics of cell-cell signaling and its impact on single-cell differentiation

285   status is an intriguing subject for future study.

286

287   In conclusion, we present a multiplexed approach integrating long-term live imaging, automated

288   image analysis, and a unique graph-based analysis to quantify the spatial organization of neural

289   progenitors during neuronal differentiation. Our method introduces a tangible means to test

290   theories about spatially-dependent forms of neural cell communication. Insights from this study

291   help further our understanding of the design principles involved in the development of functional

292   neural networks. Applications of this work can help pave the way for systematic modulation of

293   neural cell self-organization for therapeutic purposes.

294

295   **Methods**

296

297   **hNPC culture.** Human neural progenitor cells (hNP1^{TM}) derived from H9 human embryonic

298   stem cells were obtained from ArunA Biomedicals (Athens, GA). Cells were expanded on tissue

299   culture flasks pre-coated with either fibronectin (Sigma-Aldrich) or Matrigel (BD Biosciences), in

300   proliferation medium consisting of AB2^{TM} basal neural medium, ANS^{TM} neural supplement (both

301   supplied by manufacturer), 10 ng/ml leukemia inhibitory factor (LIF; EMD Millipore), 20 ng/ml

302   basic fibroblast growth factor (bFGF; R&D Systems) and 2 mM GlutaMAX^{TM} supplement (Life

303   Technologies). For neuronal differentiation experiments, cells were plated on different substrates

304   pre-coated with Matrigel and cultured in differentiation medium (proliferation medium lacking

305   bFGF).

306

307   **Electrophysiology.** For whole-cell patch clamp experiments, cultures were maintained in

308   extracellular recording solution containing 119 mM NaCl, 5 mM KCl, 10 mM HEPES, 2 mM

309   CaCl$_2$ and 1mM MgCl$_2$, titrated to a pH of 7.3. Pipettes (5-10 MΩ) were pulled from standard

310 borosilicate glass capillaries and back filled with intracellular recording solution containing 8 mM

311 NaCl, 10mM KCl, 5 mM HEPES, 0.06 mM $CaCl_2$, 5 mM $MgCl_2$, 130 mM potassium gluconate

312 and 0.6mM EGTA, titrated to a pH of 7.4. Recordings were performed using a MultiClamp 700A

313 amplifier and a Digidata 1550 Data Acquisition System coupled with Clampex 10.4 software

314 (Molecular Devices). Traces were analyzed in MATLAB.

315

316 In voltage-clamp experiments, cells were held at a holding potential of -50mV and given a series

317 of voltage steps from -90 to +100 mV. In current-clamp experiments, cells were held at

318 approximately -70 mV through minimal current injection before application of a series of current

319 steps ranging from -40 to +120 pA. Magnitudes of the current steps were modified according to

320 the input resistance. Peak outward current amplitude was measured 40ms after the initiation of

321 the voltage sweep. Peak inward current was defined as the maximum transient negative current at

322 any command voltage.

323

324 **Immunocytochemistry.** For immunostaining experiments, hNPCs were plated on Matrigel-

325 coated 12 mm glass coverslips and differentiated as described above. Cultures were fixed with

326 4% paraformaldehyde for 20 min, permeabilized with 0.2% Triton-X for 5 min and blocked with

327 6% goat serum for 45 min. Primary antibodies used were mouse Nestin (1:200) and rabbit MAP2

328 (1:500). Secondary antibodies were Alexa Fluor 488 goat anti-mouse (1:1000), Alexa Fluor 594

329 goat anti-rabbit (1:1000) and cell nuclei were stained using Hoescht dye.

330

331 **Time-lapse Microscopy.** For all time-lapse imaging experiments, hNPCs were plated at

332 approximately 50% confluence on 12-well plates pre-coated with Matrigel and switched to

333 differentiation medium 24 hours post-plating. Two datasets (biological replicates) were obtained

334 by imaging the well plates at days 0, 3, 6, 9, 12 and 14 after withdrawal of bFGF from culture

335 medium, using an automated stage Nikon Eclipse Ti-E Microscope. At the start of the

336   experiment, 5 locations were chosen arbitrarily for each well, and the same locations were imaged

337   at each time point. Imaging sessions lasted about 10 minutes and the plates were returned to the

338   incubator after imaging. A third dataset was obtained through continuous imaging, for which the

339   well plate was mounted on the stage of the microscope in a bold line cage incubator (Okolabs)

340   equipped with temperature control and gas flow rate control enabling a 37^0C 5% CO_2

341   environment. For this dataset, images were acquired at 1-hour intervals for 8 days (Supplemental

342   Video 1). In all imaging experiments, 8-bit phase contrast images were acquired through a 10X

343   objective and at a resolution of 1280 x 1080 pixels. Physical pixel size was 0.64μm.

344

345   **Image Processing.** Image sequences were chosen for analysis based on the ability of a human

346   observer to distinguish cellular features in the images. Images with large amounts of debris

347   occluding cells were discarded manually. In this manner, a total of 16, 14 and 10 image

348   sequences for each of the 3 independent datasets were chosen for analysis.

349

350   The selected time-lapse image sequences were analyzed using custom-written MATLAB code.

351   Grayscale images were pre-processed by applying a median filter with a neighborhood of 3x3

352   pixels to remove noise and segmented using an unbiased intensity-gradient thresholding approach

353   (Curl et al. 2004). Starting from the grayscale image, the first derivative of the pixel intensity

354   histogram was calculated. Fitting a linear function to the ascending portion of the first derivative

355   and extrapolating to the x-axis resulted in a grayscale threshold, which was used to generate a

356   binary image distinguishing cellular features from the background. Morphological operations

357   performed on the binary image were:

358   1. Small objects of size lesser than 50 pixels were removed to filter out noise and other

359   imaging artifacts.

360   2. Morphological opening was performed using a disk structuring element of radius 4

361   pixels. This was done to separate linear features (neurites), and circular features (cell

362   bodies).

363   3. Neurites were skeletonized using the bwmorph function in MATLAB to obtain neurite

364   length statistics.

365   4. Cell bodies were separated using connected component labeling using the default 8-

366   connected neighborhood.

367   5. Cell body objects smaller than 150 pixels and those touching the image border were

368   removed.

369   All parameters used in image processing are listed in Table S1.

370

371   In order to quantify the accuracy of our image processing algorithms, we compared the results

372   with manual tracing of soma. These results showed a close agreement between the numbers of

373   cells detected by our algorithm and by manual tracing at different time points (Supplemental

374   Figure 1).

375

376   **Graph Representation of Microscope Images.** For each pair of soma, a threshold distance for

377   proximity was defined as the average of the two soma diameters, multiplied by a scaling factor

378   (S). If the Euclidean distance between the soma centroids was lower than the threshold distance

379   computed, then the pair of soma was connected with a "proximity edge" (Figure 3E-G).

380

381   In order to capture changes in network structure across a 14-day period of differentiation, we

382   chose to use label-free phase contrast imaging (Weber et al. 2013). Immunostaining or the use of

383   fluorescent reporters would have resulted in images with better signal-to-noise to aid in image

384   analysis, but we chose to avoid these methods due to the inability to perform longitudinal imaging

385   without harming cell health. Due to the limits of our imaging method, automated image

386   segmentation often detected a smaller region than the exact cell boundary. In order to compensate

387   for this, we used a scaling factor to define spatial proximity for graph representations. Small

388   values of the scaling factor (1<S<2) resulted in sparse graphs, where interpretation of metrics

389   became difficult. Higher values of the scaling factor (2<S<3) resulted in qualitatively similar

390   results (Supplemental Figure 2), and we therefore chose S = 2 as the default scaling factor.

391

392   **Metric Computation.** All the network metrics described in Table 1 were computed using

393   custom-written code, building upon the routines provided in (Bounova and De Weck 2012). In

394   addition, some parameters like connected components and path lengths were computed using

395   built-in MATLAB functions.

396

397   Random graphs were constructed through degree-preserving rewiring, maintaining the degree

398   distribution of the original graph (Supplemental Figure 3). Each link (edge) belonging to any

399   given node in the original graph was randomly re-assigned to a node that was chosen from all

400   possible nodes with uniform probability. Metrics computed for random graphs were averaged

401   across 100 different realizations of the random graphs. This mode of random graph generation

402   was chosen to eliminate finite-size effects inherent in other models of random graphs such as

403   Erdõs-Rényi random graphs.

404

405   To ensure robustness of the network metrics, we tested varying fields of view for the images, and

406   confirmed the trends remained consistent (Supplemental Figure 5).

407   **Statistical Analyses.** Data are presented as means ± S.E.M. of a minimum of 3 experiments,

408   unless indicated otherwise. Student t-test was performed to analyze peak currents in

409   electrophysiology experiments, with significance accepted at *P < 0.05.

410

Acknowledgements

Author Contributions

All authors designed the experiments. A.S.M. performed the experiments. A.A.Q. and A.S.M. analyzed the data. All authors contributed to writing the manuscript. A.A.Q. and J.T.R. supervised the work.

References

Abranches, Elsa, Margarida Silva, Laurent Pradier, Herbert Schulz, Oliver Hummel, Domingos Henrique, and Evguenia Bekman. 2009. "Neural Differentiation of Embryonic Stem Cells in Vitro: A Road Map to Neurogenesis in the Embryo." *PLoS ONE* 4 (7). doi:10.1371/journal.pone.0006286.

Andersson, Emma R, Rickard Sandberg, and Urban Lendahl. 2011. "Notch Signaling: Simplicity in Design, Versatility in Function." *Development (Cambridge, England)* 138 (17): 3593–3612. doi:10.1242/dev.063610.

Androutsellis-Theotokis, Andreas, Ronen R Leker, Frank Soldner, Daniel J Hoeppner, Rea Ravin, Steve W Poser, Maria a Rueger, Soo-Kyung Bae, Raja Kittappa, and Ronald D G McKay. 2006. "Notch Signalling Regulates Stem Cell Numbers in Vitro and in Vivo." *Nature* 442 (August): 823–26. doi:10.1038/nature04940.

Bertrand, Nicolas, and Nadia Dahmane. 2006. "Sonic Hedgehog Signaling in Forebrain Development and Its Interactions with Pathways That Modify Its Effects." *Trends in Cell Biology* 16 (11): 597–605. doi:10.1016/j.tcb.2006.09.007.

Blankenship, Aaron G, and Marla B Feller. 2010. "Mechanisms Underlying Spontaneous Patterned Activity in Developing Neural Circuits." *Nature Reviews. Neuroscience* 11 (1).

442   Nature Publishing Group: 18–29. doi:10.1038/nrn2759.

443 Bounova, Gergana, and Olivier De Weck. 2012. "Overview of Metrics and Their Correlation
444   Patterns for Multiple-Metric Topology Analysis on Heterogeneous Graph Ensembles."
445   *Physical Review E - Statistical, Nonlinear, and Soft Matter Physics* 85.
446   doi:10.1103/PhysRevE.85.016117.

447 Bullmore, Ed, Ed Bullmore, Olaf Sporns, and Olaf Sporns. 2009. "Complex Brain Networks:
448   Graph Theoretical Analysis of Structural and Functional Systems." *Nat Rev Neurosci* 10
449   (maRcH): 186–98. doi:10.1038/nrn2575.

450 Butt, Simon J.B., Marc Fuccillo, Susana Nery, Steven Noctor, Arnold Kriegstein, Joshua G.
451   Corbin, and Gord Fishell. 2005. "The Temporal and Spatial Origins of Cortical Interneurons
452   Predict Their Physiological Subtype." *Neuron* 48 (4): 591–604.
453   doi:10.1016/j.neuron.2005.09.034.

454 Cohen, Andrew R, Francisco L a F Gomes, Badrinath Roysam, and Michel Cayouette. 2010.
455   "Computational Prediction of Neural Progenitor Cell Fates." *Nature Methods* 7 (3). Nature
456   Publishing Group: 213–18. doi:10.1038/nmeth.1424.

457 Colizza, Vittoria, Alessandro Flammini, M. Angeles Serrano, and Alessandro Vespignani. 2006.
458   "Detecting Rich-Club Ordering in Complex Networks" 2 (February): 110–15.
459   doi:10.1038/nphys209.

460 Curl, ClaireL., Trudi Harris, PeterJ. Harris, BrendanE. Allman, CatherineJ. Bellair, AlastairG.
461   Stewart, and LeaM.D. Delbridge. 2004. "Quantitative Phase Microscopy: A New Tool for
462   Measurement of Cell Culture Growth and Confluency in Situ." *Pflugers Archiv - European*
463   *Journal of Physiology* 448: 462–68. doi:10.1007/s00424-004-1248-7.

464 de Santos-Sierra, Daniel, Irene Sendiña-Nadal, Inmaculada Leyva, Juan A Almendral, Sarit
465   Anava, Amir Ayali, David Papo, and Stefano Boccaletti. 2014. "Emergence of Small-World
466   Anatomical Networks in Self-Organizing Clustered Neuronal Cultures." *PloS One* 9 (1):
467   e85828. doi:10.1371/journal.pone.0085828.

468 de Santos-Sierra, Daniel, Irene Sendiña-Nadal, Inmaculada Leyva, Juan a. Almendral, Amir
469   Ayali, Sarit Anava, Carmen Sánchez-Ávila, and Stefano Boccaletti. 2014. "Graph-Based
470   Unsupervised Segmentation Algorithm for Cultured Neuronal Networks' Structure
471   Characterization and Modeling." *Cytometry Part A*, n/a – n/a. doi:10.1002/cyto.a.22591.

472 Downes, Julia H, Mark W Hammond, Dimitris Xydas, Matthew C Spencer, Victor M Becerra,
473   Kevin Warwick, Ben J Whalley, and Slawomir J Nasuto. 2012. "Emergence of a Small-
474   World Functional Network in Cultured Neurons." *PLoS Computational Biology* 8 (5).
475   Public Library of Science: e1002522. doi:10.1371/journal.pcbi.1002522.

476 Edri, Reuven, Yakey Yaffe, Michael J Ziller, Naresh Mutukula, Rotem Volkman, Eyal David,
477   Jasmine Jacob-Hirsch, et al. 2015. "Analysing Human Neural Stem Cell Ontogeny by
478   Consecutive Isolation of Notch Active Neural Progenitors." *Nature Communications* 6
479   (January). Nature Publishing Group: 6500. doi:10.1038/ncomms7500.

480 Feldt, Sarah, Paolo Bonifazi, and Rosa Cossart. 2011. "Dissecting Functional Connectivity of
481   Neuronal Microcircuits: Experimental and Theoretical Insights." *Trends in Neurosciences*
482   34 (5): 225–36. doi:10.1016/j.tins.2011.02.007.

483 ffrench-Constant. 2008. "The Neural Stem Cell Microenvironment." *StemBook*, 1–26.
484   doi:10.3824/stembook.1.15.1.

485 Friedl, Peter, and Darren Gilmour. 2009. "Collective Cell Migration in Morphogenesis,

486   Regeneration and Cancer." *Nature Reviews Molecular Cell Biology* 10 (7). Nature
487   Publishing Group: 445–57. doi:10.1038/nrm2720.

488 Gage, F. H. 2000. "Mammalian Neural Stem Cells." *Science* 287 (5457): 1433–38.
489   doi:10.1126/science.287.5457.1433.

490 Gage, Fred H., and Sally Temple. 2013. "Neural Stem Cells: Generating and Regenerating the
491   Brain." *Neuron* 80 (3). Elsevier Inc.: 588–601. doi:10.1016/j.neuron.2013.10.037.

492 Guillemot, François. 2007. "Spatial and Temporal Specification of Neural Fates by Transcription
493   Factor Codes." *Development (Cambridge, England)* 134: 3771–80.
494   doi:10.1242/dev.006379.

495 Hallett, Penelope J., Oliver Cooper, Damaso Sadi, Harold Robertson, Ivar Mendez, and Ole
496   Isacson. 2014. "Long-Term Health of Dopaminergic Neuron Transplants in Parkinson's
497   Disease Patients." *Cell Reports* 7 (6). The Authors: 1755–61.
498   doi:10.1016/j.celrep.2014.05.027.

499 Imayoshi, Itaru, Akihiro Isomura, Yukiko Harima, Kyogo Kawaguchi, Hiroshi Kori, Hitoshi
500   Miyachi, Takahiro Fujiwara, Fumiyoshi Ishidate, and Ryoichiro Kageyama. 2013.
501   "Oscillatory Control of Factors Determining Multipotency and Fate in Mouse Neural
502   Progenitors." *Science (New York, N.Y.)* 342 (2013): 1203–8. doi:10.1126/science.1242366.

503 Imayoshi, Itaru, and Ryoichiro Kageyama. 2014. "bHLH Factors in Self-Renewal, Multipotency,
504   and Fate Choice of Neural Progenitor Cells." *Neuron* 82 (1). Elsevier Inc.: 9–23.
505   doi:10.1016/j.neuron.2014.03.018.

506 Kageyama, Ryoichiro, Toshiyuki Ohtsuka, Hiromi Shimojo, and Itaru Imayoshi. 2009. "Dynamic
507   Regulation of Notch Signaling in Neural Progenitor Cells." *Current Opinion in Cell Biology*
508   21: 733–40. doi:10.1016/j.ceb.2009.08.009.

509 Malmersjö, Seth, Paola Rebellato, Erik Smedler, Henrike Planert, Shigeaki Kanatani, Isabel Liste,
510   Evanthia Nanou, et al. 2013. "Neural Progenitors Organize in Small-World Networks to
511   Promote Cell Proliferation." *Proceedings of the National Academy of Sciences of the United*
512   *States of America* 110: E1524–32. doi:10.1073/pnas.1220179110.

513 Mason, Ivor. 2007. "Initiation to End Point: The Multiple Roles of Fibroblast Growth Factors in
514   Neural Development." *Nature Reviews. Neuroscience* 8 (July): 583–96.
515   doi:10.1038/nrn2189.

516 Newman, M. 2002. "Assortative Mixing in Networks." *Physical Review Letters* 89 (20): 208701.
517   doi:10.1103/PhysRevLett.89.208701.

518 Pfeuty, B. 2015. "A Computational Model for the Coordination of Neural Progenitor Self-
519   Renewal and Differentiation through Hes1 Dynamics." *Development* 142: 477–85.
520   doi:10.1242/dev.112649.

521 Rosado-de-Castro, Paulo Henrique, Pedro Moreno Pimentel-Coelho, Lea Mirian Barbosa da
522   Fonseca, Gabriel Rodriguez de Freitas, and Rosalia Mendez-Otero. 2013. "The Rise of Cell
523   Therapy Trials for Stroke: Review of Published and Registered Studies." *Stem Cells and*
524   *Development* 22 (15). Mary Ann Liebert, Inc. 140 Huguenot Street, 3rd Floor New
525   Rochelle, NY 10801 USA: 2095–2111. doi:10.1089/scd.2013.0089.

526 Schroeder, Timm. 2011. "Long-Term Single-Cell Imaging of Mammalian Stem Cells." *Nature*
527   *Methods* 8 (4 Suppl): S30–35. doi:10.1038/nmeth.1577.

528 Shefi, Orit, Eshel Ben-Jacob, and Amir Ayali. 2002. "Growth Morphology of Two-Dimensional

Insect Neural Networks." *Neurocomputing* 44-46: 635–43. doi:10.1016/S0925-2312(02)00451-4.

Shefi, Orit, Ido Golding, Ronen Segev, Eshel Ben-Jacob, and Amir Ayali. 2002. "Morphological Characterization of in Vitro Neuronal Networks." *Physical Review E* 66 (2): 1–5. doi:10.1103/PhysRevE.66.021905.

Shen, Qin, Yue Wang, John T Dimos, Christopher a Fasano, Timothy N Phoenix, Ihor R Lemischka, Natalia B Ivanova, Stefano Stifani, Edward E Morrisey, and Sally Temple. 2006. "The Timing of Cortical Neurogenesis Is Encoded within Lineages of Individual Progenitor Cells." *Nature Neuroscience* 9 (6): 743–51. doi:10.1038/nn1694.

Shimojo, Hiromi, Toshiyuki Ohtsuka, and Ryoichiro Kageyama. 2008. "Oscillations in Notch Signaling Regulate Maintenance of Neural Progenitors." *Neuron* 58: 52–64. doi:10.1016/j.neuron.2008.02.014.

Spitzer, Nicholas C. 2006. "Electrical Activity in Early Neuronal Development." *Nature* 444 (7120): 707–12. doi:10.1038/nature05300.

Sun, Bo, Josephine Lembong, Valery Normand, Matthew Rogers, and Howard A Stone. 2012. "Spatial-Temporal Dynamics of Collective Chemosensing." *Proceedings of the National Academy of Sciences of the United States of America* 109 (20): 7753–58. doi:10.1073/pnas.1121338109.

Watters, Andrea K, Slava Rom, Jeremy D Hill, Marie K Dematatis, Yu Zhou, Steven F Merkel, Allison M Andrews, et al. 2015. "Identification and Dynamic Regulation of Tight Junction Protein Expression in Human Neural Stem Cells." *Stem Cells and Development* 24 (12): 1377–89. doi:10.1089/scd.2014.0497.

Weber, Sebastian, María L. Fernández-Cachón, Juliana M. Nascimento, Steffen Knauer, Barbara Offermann, Robert F. Murphy, Melanie Boerries, and Hauke Busch. 2013. "Label-Free Detection of Neuronal Differentiation in Cell Populations Using High-Throughput Live-Cell Imaging of PC12 Cells." *PLoS ONE* 8 (2). doi:10.1371/journal.pone.0056690.

Wilson, Patricia G, and Steve S Stice. 2006. "Development and Differentiation of Neural Rosettes Derived from Human Embryonic Stem Cells." *Stem Cell Reviews* 2 (1): 67–77. doi:10.1007/s12015-006-0011-1.

Yu, Yong-Chun, Ronald S Bultje, Xiaoqun Wang, and Song-Hai Shi. 2009. "Specific Synapses Develop Preferentially among Sister Excitatory Neurons in the Neocortex." *Nature* 458 (7237). Macmillan Publishers Limited. All rights reserved: 501–4. doi:10.1038/nature07722.

Zhou, Zhi-Dong, Udhaya Kumari, Zhi-Cheng Xiao, and Eng-King Tan. 2010. "Notch as a Molecular Switch in Neural Stem Cells." *IUBMB Life* 62 (8): 618–23. doi:10.1002/iub.362.